

# *Ab initio* insight into ultrafast nonadiabatic decay of hypoxanthine: keto-N7H and keto-N9H tautomers†

Cite this: *Phys. Chem. Chem. Phys.*, 2013, **15**, 10777

Xugeng Guo,<sup>a</sup> Zhenggang Lan<sup>\*b</sup> and Zexing Cao<sup>\*a</sup>

Nonadiabatic dynamics simulations at the SA-CASSCF level were performed for the two most stable keto-N7H and keto-N9H tautomers of hypoxanthine in order to obtain deep insight into the lifetime of the optically bright  $S_1(^1\pi\pi^*)$  excited state and the relevant decay mechanisms. Supporting calculations on the ground-state ( $S_0$ ) equilibrium structures and minima on the crossing seams of both tautomers were carried out at the MR-CIS and CASSCF levels. These studies indicate that there are four slightly different kinds of conical intersections in each tautomer, exhibiting a chiral character, each of which dominates a barrierless reaction pathway. Moreover, both tautomers reveal the ultrafast  $S_1 \rightarrow S_0$  decay, in which the  $S_1$  state of keto-N9H in the gas phase has a lifetime of 85.5 fs, whereas that of keto-N7H has a longer lifetime of 137.7 fs. An excellent agreement is found between the present results and the experimental value of  $130 \pm 20$  fs in aqueous solution (Chen and Kohler, *Phys. Chem. Chem. Phys.*, 2012, **14**, 10677–10689).

Received 31st December 2012,  
Accepted 19th April 2013

DOI: 10.1039/c3cp44718a

www.rsc.org/pccp

## 1 Introduction

This work was motivated by the detection of the ultrafast deactivation in the rare natural nucleobase hypoxanthine, by means of femtosecond time-resolved spectroscopies and the desire to elucidate theoretically the underlying mechanisms.<sup>1–3</sup> It has been widely accepted that upon UV radiation, this ultrafast decay acts as a protection mechanism, which can significantly reduce the probability of undergoing photochemical reactions in the photoexcited states. For this reason, the unique photostability of hypoxanthine and its derivatives has been intensively investigated in a number of laboratories and by the quantum-chemical calculations.<sup>1–22</sup>

Experimentally, Röttger *et al.* reported a comprehensive study on the excited-state dynamics of hypoxanthine in aqueous solution at pH = 7 by using different time-resolved spectroscopies.<sup>1</sup> They observed the presence of three different time constants ( $\tau_1 \leq 0.10$  ps,  $\tau_2 = 0.21 \pm 0.08$  ps, and  $\tau_3 = 1.80 \pm 0.40$  ps) and assigned

the second one as the lifetime of the first  $S_1(^1\pi\pi^*)$  excited state.<sup>1</sup> In light of the observed evidence, they thus proposed a tentative relaxation mechanism, and it is assumed that after  $^1\pi\pi^*$  photo-excitation the molecule proceeds through an  $S_1/S_0$  conical intersection on a direct and barrierless pathway and then returns to the ground electronic state ( $S_0$ ).<sup>1</sup> Villabona-Monsalve *et al.* later recorded the fluorescence lifetimes of hypoxanthine with the femtosecond fluorescence up-conversion technique, in which both predominant keto-N7H and keto-N9H tautomers (see Fig. 1) reveal

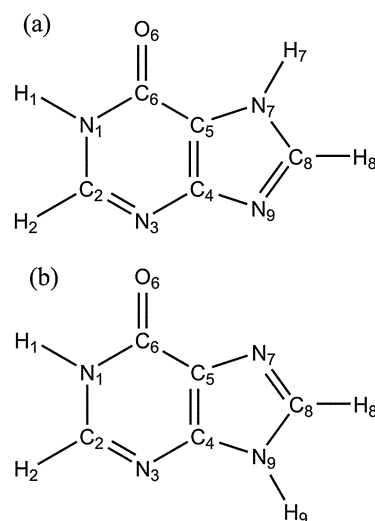


Fig. 1 Molecular structures and atom numbering of keto-N7H (a) and keto-N9H (b).

<sup>a</sup> State Key Laboratory for Physical Chemistry of Solid Surfaces and Fujian Provincial Key Lab of Theoretical and Computational Chemistry, College of Chemistry and Chemical Engineering, Xiamen University, Xiamen 361005, P.R. China. E-mail: zxciao@xmu.edu.cn

<sup>b</sup> Qingdao Key Laboratory of Solar Energy Utilization and Energy Storage Technology, Qingdao Institute of Bioenergy and Bioprocess Technology, Chinese Academy of Sciences, Qingdao, 266101, P.R. China. E-mail: lanzg@qibebt.ac.cn

† Electronic supplementary information (ESI) available: Schematic plots of active orbitals in keto-N7H and keto-N9H. Minima on the crossing seams with  $^2E$  conformation of keto-N7H and keto-N9H. Percentages of each type of intersection structures of keto-N9H. Time evolution of the  $S_1$  state average population in keto-N7H and keto-N9H along with the fitting parameters. Cartesian coordinates of the optimized geometries. See DOI: 10.1039/c3cp44718a

ultrashort excited-state lifetimes ( $\tau < 0.20$  ps) in a pH 5 aqueous solution.<sup>2</sup> Shortly thereafter, Chen and Kohler gained a shorter lifetime of  $\tau = 0.13 \pm 0.20$  ps with the femtosecond transient absorption spectroscopy in aqueous solution.<sup>3</sup>

Concerning theoretical investigations, many quantum-chemical approaches, including TD-B3LYP,<sup>18</sup> MCQDPT2,<sup>19</sup> MRMP2,<sup>2,20</sup> and MR-CIS,<sup>2</sup> have been devoted to characterizing the absorption spectra and conical intersections of hypoxanthine. For example, the conical intersections between the  $S_1$  and  $S_0$  states of keto-N7H and keto-N9H calculated by Villabona-Monsalve *et al.* at the MR-CIS level show envelope-like structures puckering at the  $C_2$  atom ( $E_2$  conformation, see Fig. 1 for the atom numbering).<sup>2</sup> Although there are so many important contributions, excited-state dynamics simulations have never been carried out for the two dominant tautomers of hypoxanthine to our knowledge. Because of the approximately equal population in water (53–54% for keto-N7H),<sup>2</sup> a detailed theoretical investigation is necessary to address some of the key issues: (i) what role does the tautomerism in N7H and N9H forms play in the nonadiabatic decay process? (ii) Are both tautomers responsible for the ultrafast decay observed in experiments? (iii) Do both tautomers exhibit the similar decay mechanisms? (iv) And, can the above  $E_2$  conical intersections be activated on the less than 200 fs time scale proposed by Villabona-Monsalve *et al.*?<sup>2</sup> Herein we employed sophisticated methods, such as CASSCF and MR-CIS, in the framework of the state-of-the-art surface-hopping dynamics approach to understand in depth the excited-state lifetimes and deactivation mechanisms of the two targeted molecules.

## 2 Computational details

The geometry optimizations for the  $S_0$  states of the keto-N7H and keto-N9H tautomers were explored by the restricted-spin coupled-cluster singles and doubles (CCSD)<sup>23</sup> approach with a  $C_s$ -symmetry constraint as well as the multireference configuration interaction with single excitations (MR-CIS) and complete active space self-consistent-field (CASSCF) methods without a symmetry constraint. The active space in the MR-CIS and CASSCF calculations was composed by ten electrons in eight orbitals including five  $\pi$  and three  $\pi^*$ . This particular choice of active space provides a balanced description of computational cost and accuracy and can treat the lowest-lying optically allowed  $S_1(^1\pi\pi^*)$  excited states more effectively (see below for the comparison with other calculations). In addition, the minima on the crossing seams between  $S_1$  and  $S_0$  states were also optimized at the MR-CIS and CASSCF levels of theory. Two electronic states were involved in the state-averaging procedure (SA-2), and the 6-31G(d) basis set was employed for all atoms.

The vertical excitation energies of  $S_1(^1\pi\pi^*)$  states of keto-N7H and keto-N9H were computed by the complete active space second-order perturbation theory (CASPT2)<sup>24,25</sup> method with a cc-pVTZ basis set at the CCSD equilibrium geometries. In the gas phase, two sets of active spaces were used: CASPT2(10,8) and CASPT2(10,9), where an additional  $\pi^*$  orbital was incorporated into the active space of the latter. In aqueous solution,

only CASPT2(10,9) calculations were performed in combination with the polarizable continuum model (PCM) so as to moderate the effect of the intruder states. Additionally, the MR-CIS(10,8)/6-31G(d) results were also listed for a direct comparison.

Mixed quantum-classical dynamics simulations for keto-N7H and keto-N9H were performed by the fewest switches surface-hopping approach<sup>26</sup> at the SA-2-CASSCF(10,8) level. For each tautomer, two hundred trajectories starting at the  $S_1(^1\pi\pi^*)$  state were calculated and the maximum simulation time was 300 fs. However, trajectories that evolved into the  $S_0$  state and stayed there for more than 100 fs were terminated. The classical equations were integrated using the velocity-Verlet algorithm<sup>27</sup> with a constant time step of 0.5 fs. Initial conditions were generated based on the harmonic oscillator Wigner distribution<sup>28,29</sup> for the  $S_0$  state. Further technical details on the dynamics calculations can be seen in previous contributions.<sup>30–34</sup>

The CCSD calculations were performed using the MOLPRO 2009 package.<sup>35</sup> The MR-CIS and CASSCF calculations were carried out with the COLUMBUS package.<sup>36–38</sup> The CASPT2 calculations were performed using the MOLCAS 7.4 program.<sup>39</sup> The nonadiabatic dynamics simulations were implemented with the NEWTON-X program<sup>40,41</sup> using the analytical gradients<sup>42–44</sup> and nonadiabatic coupling vectors<sup>45,46</sup> provided by COLUMBUS.

## 3 Results and discussion

### 3.1 $S_0$ equilibrium geometries and vertical transition energies

In hypoxanthine, keto-N7H and keto-N9H are the two most stable tautomers,<sup>10,17</sup> with the former being  $\sim 0.25$  kcal mol<sup>−1</sup> lower in energy than the latter in the gas phase at their CCSD optimized structures. This indicates that both tautomers can exist in almost equal amounts at room temperature, which is consistent with the experimental finding as mentioned above.<sup>2</sup> All computational approaches considered here predict that the ground-state structures ( $S_0$ -MIN) of both tautomers are planar with  $C_s$  symmetry. The optimized key geometric parameters are summarized in Table 1, and Cartesian coordinates are provided in the ESI† (Tables S1–S6). It is noticeable that the CCSD, MR-CIS, and CASSCF results are quite close to one another, suggesting that the active space employed in the current MR-CIS and CASSCF calculations is reasonably reliable.

The previous MRMP2 calculations<sup>2</sup> have demonstrated that for keto-N7H and keto-N9H, the first excited singlet state ( $S_1$ ) is of  $\pi\pi^*$  character, followed by an optically dark  $S_2(n\pi^*)$  state, and the energy gaps of two excited states are 0.24 and 0.77 eV, respectively. This means that the  $n\pi^*$  state will not play a significant role in the nonadiabatic decay process. Since this work follows with interest the deactivation pathway of the  $S_1(^1\pi\pi^*)$  state, we only discuss the vertical transition energies to this lowest singlet excited state (see Table 2). The  $S_1(^1\pi\pi^*)$  state arises from single electron promotion from the highest-occupied molecular orbital (HOMO) to the lowest-unoccupied molecular orbital (LUMO), and the HOMO and LUMO schematic plots can be seen in the ESI† (see Fig. S1). As shown in Table 2, the  $S_1(^1\pi\pi^*)$  states of keto-N7H and keto-N9H at the CASPT2 level are predicted to be at 4.85 and 4.60 eV in the gas phase,

**Table 1** Primary bond lengths (in angstroms) and dihedral angles (in degrees) in the optimized geometries of keto-N7H and keto-N9H

Geom.	Conf.	C <sub>4</sub> C <sub>5</sub>	N <sub>7</sub> C <sub>8</sub>	C <sub>8</sub> N <sub>9</sub>	C <sub>4</sub> N <sub>3</sub> C <sub>2</sub> N <sub>1</sub>	C <sub>6</sub> N <sub>1</sub> C <sub>2</sub> N <sub>3</sub>	C <sub>4</sub> N <sub>3</sub> C <sub>2</sub> H <sub>2</sub>
keto-N7H							
S <sub>0</sub> -MIN <sup>a</sup>		1.386	1.366	1.320	0.0	0.0	180.0
S <sub>0</sub> -MIN <sup>b</sup>		1.393	1.356	1.320	0.0	0.0	180.0
S <sub>0</sub> -MIN <sup>c</sup>		1.374	1.357	1.306	0.0	0.0	180.0
Ethylenic I <sup>b</sup>	E <sub>2</sub>	1.414	1.357	1.319	−66.7	65.1	82.2
Ethylenic II <sup>b</sup>	E <sub>2</sub>	1.432	1.363	1.312	−75.5	74.9	111.5
Prev. work <sup>d</sup>	E <sub>2</sub>	1.402			−69.1	66.4	
keto-N9H							
S <sub>0</sub> -MIN <sup>a</sup>		1.386	1.312	1.379	0.0	0.0	180.0
S <sub>0</sub> -MIN <sup>b</sup>		1.392	1.311	1.368	0.0	0.0	180.0
S <sub>0</sub> -MIN <sup>c</sup>		1.372	1.298	1.369	0.0	0.0	180.0
Ethylenic I <sup>b</sup>	E <sub>2</sub>	1.417	1.312	1.376	−67.9	68.5	86.0
Ethylenic II <sup>b</sup>	E <sub>2</sub>	1.437	1.314	1.373	−75.1	77.0	113.0
Prev. work <sup>d</sup>	E <sub>2</sub>	1.447			−73.1	75.6	

<sup>a</sup> CCSD/6-31G(d). <sup>b</sup> MR-CIS(10,8)/6-31G(d). <sup>c</sup> CASSCF(10,8)/6-31G(d).  
<sup>d</sup> MR-CIS(12,9)/cc-pVDZ.<sup>2</sup>

respectively, which agree very well with the available experimental observations and previous theoretical calculations.<sup>2,4,18–20</sup> Although the MR-CIS calculations overestimate the transition energies by about 1 eV, their predicted energy difference between both tautomers is only 0.11 eV, which is compatible with the CASPT2(10,8) (0.25 eV) and MRMP2 (0.16 eV) results.<sup>2</sup>

To estimate the solvent effect on the excited-state properties, CASPT2(10,9) calculations in combination with the PCM approach were performed. CASPT2(10,9)-predicted vertical excitation energies in the gas phase and in aqueous solution, along with available experimental values from 9-methyl-hypoxanthine,<sup>4</sup> are compiled into Table 3. We note that the solvent effect results in a red shift of 0.04 eV and a blue shift of 0.06 eV for the vertical transition energies in keto-N7H and keto-N9H, respectively, which is comparable to the experimental blue shift of 0.18 eV. Accordingly, the solvent effect on the excited state is not remarkable here. Recently, Thiel and co-workers explored the ultrafast nonadiabatic decay of the 9H-guanine analogue in the gas phase and aqueous solution, and they found that the excited-state lifetimes in the gas phase and in solution are comparable.<sup>47,48</sup>

### 3.2 S<sub>1</sub>/S<sub>0</sub> conical intersections

Minima on the crossing seams (MXSs) between the S<sub>1</sub> and S<sub>0</sub> states of the keto-N7H and keto-N9H tautomeric forms are depicted in Fig. 2, and the main geometrical parameters are also listed in Table 1, together with the previous MR-CIS(12,9) results.<sup>2</sup> It should be noted that the mirror structures of the above S<sub>1</sub>/S<sub>0</sub> MXSs should also exist due to chirality. The reversed

**Table 3** CASPT2(10,9)-calculated vertical transition energies ( $\Delta E$ , in eV) and oscillator strengths ( $f$ ) of keto-N7H and keto-N9H in the gas phase (in plain) and in aqueous solution (in italic)

Species	$\Delta E$	$f$	Expt. <sup>a</sup>
keto-N7H	4.79	0.122	
	<i>4.75</i>	<i>0.128</i>	
keto-N9H	4.58	0.167	4.41
	<i>4.64</i>	<i>0.175</i>	4.59

<sup>a</sup> Experimental values in the vapor gas and water at pH = 6.1 from 9-methyl-hypoxanthine.<sup>4</sup>

MXSs (<sup>2</sup>E conformation) and the related Cartesian coordinates are given in the ESI† (Fig. S2 and Tables S7–S22). We note that the structures of the MXSs for keto-N7H and keto-N9H are very similar, which implies that both tautomers may have analogous photophysical properties as can be seen in the subsequent dynamics simulations.

As displayed in Fig. 2, there are two slightly different kinds of conical intersections (CIs) in each tautomer. One CI (denoted *ethylenic I*) shows an envelope-like structure with an out-of-plane distortion of the C<sub>2</sub> atom (E<sub>2</sub> conformation), and the C<sub>2</sub>–H<sub>2</sub> bonds are nearly perpendicular to the rings with the dihedral angles  $\delta(\text{C}_4\text{--N}_3\text{--C}_2\text{--H}_2)$  of 82.2 and 86.0° at the MR-CIS(10,8) level, respectively. The other CI (denoted *ethylenic II*) also exhibits an envelope puckering at the C<sub>2</sub> atom with a relatively small out-of-plane displacement and the MR-CIS(10,8) predicted dihedral angles  $\delta(\text{C}_4\text{--N}_3\text{--C}_2\text{--H}_2)$  are 111.5 and 113.0°, respectively. At the present MR-CIS(10,8) level, the potential energies of the *ethylenic I* intersections (4.35 eV for keto-N7H and 4.38 eV for keto-N9H) relative to S<sub>0</sub>-MIN are somewhat lower than those of the *ethylenic II* ones (4.58 eV for keto-N7H and 4.56 eV for keto-N9H), while the two CIs are much lower in energy than the S<sub>1</sub> states at the Franck–Condon region (see Table 2). It is thus clear that access to the two types of CIs should be possible. A similar behavior has also been found in the studies of a 9H-guanine analogue.<sup>32,47,48</sup> For instance, the *ethylenic I* and *ethylenic II* intersections predicted by Barbatti *et al.*<sup>32</sup> locate at 4.07 and 4.30 eV, respectively, and their energy gap of 0.23 eV is in accordance with our results (0.23 eV for keto-N7H and 0.18 eV for keto-N9H). On the other hand, both MR-CIS and CASSCF methods predict that <sup>2</sup>E and E<sub>2</sub> conformations are equivalent, indeed revealing a chiral character.

Obviously, the structure of the *ethylenic I* intersection for keto-N7H is in accordance with that calculated by the previous MR-CIS(12,9) method, where a lone-pair localized at the O atom (*n*<sub>O</sub>) was incorporated into the active space of the latter.<sup>2</sup> At the MR-CIS(10,8)

**Table 2** Vertical transition energies (in eV) to the S<sub>1</sub> excited states of keto-N7H (first row) and keto-N9H (second row) tautomers in the gas phase, with oscillator strengths given in parentheses

CASPT2(10,8) <sup>a</sup>	MR-CIS(10,8) <sup>b</sup>	MRMP2 <sup>c</sup>	MRMP2 <sup>d</sup>	MCQDPT2 <sup>e</sup>	TD-B3LYP <sup>f</sup>	Expt. <sup>g</sup>	Expt. <sup>h</sup>
4.85 (0.138)	5.65 (0.096)	4.64					
4.60 (0.191)	5.54 (0.198)	4.49	4.61	4.63	4.75	4.98	4.41

<sup>a</sup> CCSD/6-31G(d) geometry. <sup>b</sup> MR-CIS(10,8)/6-31G(d) geometry. <sup>c</sup> MP2/cc-pVDZ geometry. <sup>d</sup> MP2/cc-pVDZ geometry. <sup>e</sup> MP2/6-311++G(d,p) geometry. <sup>f</sup> B3LYP/6-311++G(d,p) geometry. <sup>g</sup> Experimental value in water at pH 5. <sup>h</sup> Experimental value in the vapor phase for 9-methyl-hypoxanthine.<sup>4</sup>

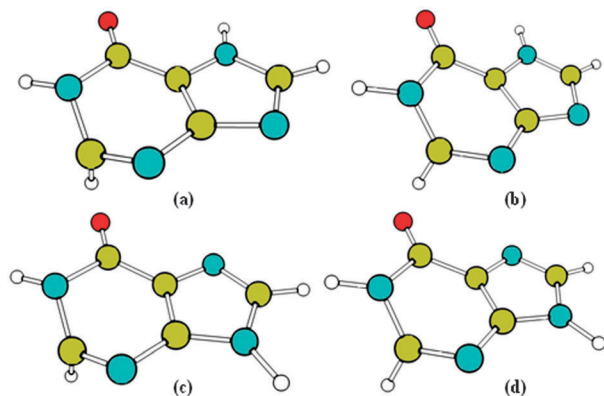


**Fig. 2** Minima on the crossing seams (MXSs) between the  $S_1$  and  $S_0$  states of keto-N7H and keto-N9H ( $E_2$  conformation). (a) (c): *Ethylenic I*; (b) (d): *ethylenic II*.

level, the main geometrical variations with respect to the MR-CIS(12,9) results are the elongation of the  $C_4-C_5$  bond by 0.012 Å and the simultaneous decrease of the dihedral angles  $\delta(C_4-N_3-C_2-N_1)$  and  $\delta(C_6-N_1-C_2-N_3)$  by 2.4 and 1.3°, respectively. However, we find that the MR-CIS(12,9) predicted structure<sup>2</sup> for keto-N9H accounts for the second type of CI (*ethylenic II*), in which the  $C_4-C_5$  bond is stretched by 0.010 Å and the dihedral angles  $\delta(C_4-N_3-C_2-N_1)$  and  $\delta(C_6-N_1-C_2-N_3)$  are reduced by 2.0 and 1.4°, respectively, in comparison to our MR-CIS(10,8) data. This further justifies the use of our small active space in the present calculations.

It is worthy of note that unconstrained geometry optimization of the  $S_1(^1\pi\pi^*)$  state starting from  $S_0$  minimum structure leads directly to a  $S_1/S_0$  conical intersection. This implies that the evolution to  $S_1/S_0$  CIs after photoexcitation may be barrierless and the nonadiabatic decay should in principle be ultrafast. Such an assumption is further supported by the following dynamics simulations.

### 3.3 Excited-state dynamics

Time evolution of the average population in the two lowest electronic states from respective 200 trajectories of keto-N7H and keto-N9H molecules is plotted in Fig. 3. It can be found that after photoexcitation into the optical active state, an ultrafast  $S_1 \rightarrow S_0$  decay takes place. The  $S_1$  state is completely depopulated in less than 250 fs.

To gain the excited-state lifetime of keto-N7H, we have fitted the time-dependent population of the  $S_1$  state with a single exponential model within the timescale of 250 fs (see Fig. S3 in the ESI†):

$$f(t) = f_{10} + (1 - f_{10})\exp[-(t - \tau_{11})/\tau_{12}] \quad (1)$$

where  $f_{10}$  is the fraction of the population which does not relax to the  $S_0$  state,  $\tau_{11}$  is the initial delay or latency time, and  $\tau_{12}$  is the exponential time constant. The excited-state lifetime ( $\tau_1$ ) is the sum of  $\tau_{11}$  and  $\tau_{12}$ . The fitting process results in  $f_{10} = 0$ ,  $\tau_{11} = 59.0$  fs,  $\tau_{12} = 78.7$  fs, and  $\tau_1 = 137.7$  (correlation coefficient  $R^2 = 0.94$ ). This indicates that the dynamics of the gas phase for keto-N7H exhibits a latency time of 59.0 fs before starting a

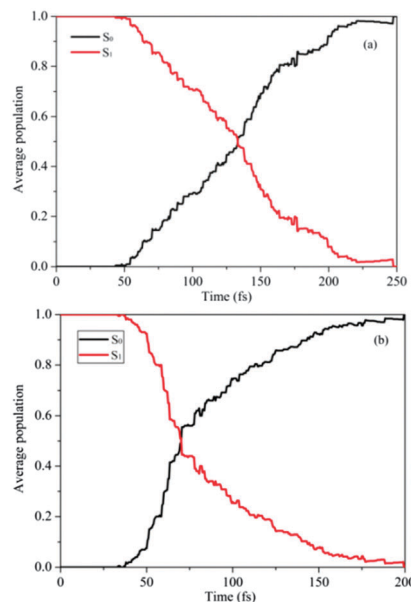


**Fig. 3** Time evolution of the average population of the  $S_1$  and  $S_0$  states from respective 200 trajectories of keto-N7H (a) and keto-N9H (b).

rapid and exponential nonadiabatic decay with a decay constant of 78.7 fs.

By fitting the  $S_1$  occupation curve of keto-N9H shown in Fig. S4 (see ESI†) with a mono-exponential function

$$f(t) = f_{20} + (1 - f_{20})\exp[-(t - \tau_{21})/\tau_{22}] \quad (2)$$

the values  $f_{20} = 0$ ,  $\tau_{21} = 42.3$  fs,  $\tau_{22} = 43.2$  fs, and  $\tau_2 = 85.5$  fs ( $R^2 = 0.99$ ) are obtained. This is also a clear indication that after an initial delay where the  $S_0$  state is not populated, the gas-phase dynamics of keto-N9H show a fast and exponential decay to the  $S_0$  state with a decay constant of 43.2 fs. It is evident that within the total 200 trajectories, the latency time of keto-N9H is somewhat shorter than that of keto-N7H (42.3 fs vs. 59.0 fs), but the exponential decay constant is strongly decreased from 78.7 to 43.2 fs, resulting in the former revealing a faster  $S_1 \rightarrow S_0$  decay than the latter (85.5 fs vs. 137.7 fs). It should be emphasized that the difference in the excited-state lifetimes between the two tautomers is not quite remarkable, indicating that the tautomerism in N7H-N9H forms have no significant effect on the nonadiabatic decay in hypoxanthine.

As mentioned in the Introduction, the dynamics of hypoxanthine in aqueous solution have recently been determined experimentally in some detail.<sup>1–3</sup> The first excited-state lifetimes recorded by Röttger *et al.*<sup>1</sup> and Villabona-Monsalve *et al.*<sup>2</sup> are very similar ( $\sim 210$  and  $\sim 200$  fs, respectively), whereas a shorter lifetime ( $\sim 130$  fs) is obtained by Chen and Kohler.<sup>3</sup> It is therefore clear that our dynamics simulations reproduce the excited-state lifetimes measured by the experiments very well. Interestingly, such a behavior in hypoxanthine is different from that of adenine, in which the N7H tautomer has an excited-state lifetime of 8.80 ps, almost fifty-times longer than that of the N9H form (0.18 ps).<sup>49</sup>

Fig. 4 shows the geometrical distribution at the  $S_1 \rightarrow S_0$  hops for keto-N7H. It is apparent that all hopping structures are

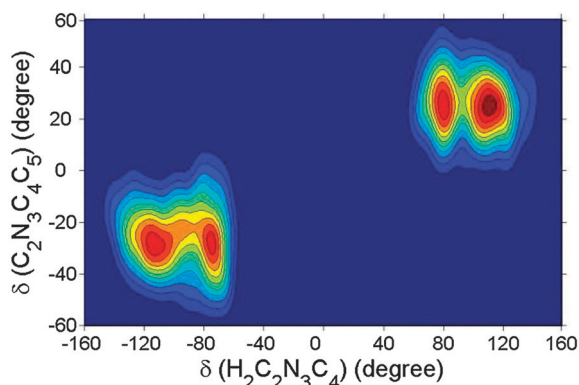


Fig. 4 Geometrical distribution at the  $S_1 \rightarrow S_0$  hops for keto-N7H.

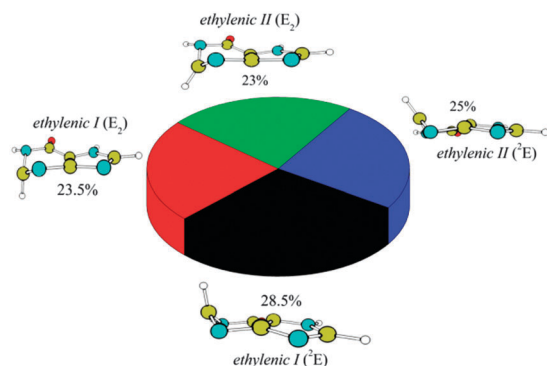


Fig. 5 Four of the main  $S_1/S_0$  conical intersections of keto-N7H. The percentages show how often each type of structure is accessed for decay in the current dynamics simulations.

divided into two almost identical parts ( $E_2$  and  ${}^2E$ ), characterized by the different signs of two dihedral angles [ $\delta(C_2-N_3-C_4-C_5)$  and  $\delta(H_2-C_2-N_3-C_4)$ ]. For each part, two CIs (*ethylenic I* and *ethylenic II*) give the similar contribution here. Overall, the number of trajectories passing each type of CI structures are essentially equal for keto-N7H (see Fig. 5). In fact the keto-N9H tautomer shows a very similar feature in its nonadiabatic dynamics, thus we put the similar figures of branching ratios into the ESI<sup>†</sup> (see Fig. S5). This statistical analysis lends support to the proposed reaction channels and relative intersections provided only by electronic-structure calculations at the MR-CIS and CASSCF levels. It should be noted that the percentage of *ethylenic II* intersections in 9H-gaunine is much larger than that of *ethylenic I* ones (67% vs. 28%) although the latter is lower in energy than the former, as mentioned above.<sup>32</sup>

## 4 Conclusions

The on-the-fly surface-hopping dynamics simulations were reported for hypoxanthine focused on its two most stable keto-N7H and keto-N9H tautomers. On the basis of calculations, we can draw several primary conclusions concerning the ground and excited state properties of both tautomers.

(1) Both keto-N7H and keto-N9H tautomers in their ground states have plane structures in  $C_s$  symmetry, with the latter being higher in energy by  $\sim 0.25$  kcal mol<sup>-1</sup> than the former in the gas phase at CCSD equilibrium geometries, which strongly supports the conclusion that both tautomers have approximately equal population in aqueous solution at room temperature (53–54% for keto-N7H).

(2) Keto-N9H exhibits a red-shifted absorption wavelength with respect to keto-N7H in the gas phase and in aqueous solution, and a good agreement is found between the calculated excitation energies and the experimental data available.

(3) There exist four somewhat different types of conical intersections in each tautomer with approximately equal branching ratios, revealing a chiral character, all of which would play the comparable role in the ultrafast nonadiabatic decay process. In addition, the similarities in conical intersection structures between both tautomers suggest that both tautomers may follow the analogous electronic decay pathways.

(4) Dynamics calculations suggest that, in the selected 200 trajectories, both tautomers show the ultrashort excited-state lifetimes, where the  $S_1({}^1\pi\pi^*)$  state of keto-N9H in the gas phase has a lifetime of 85.5 fs, about 52.2 fs shorter than that of keto-N7H. In light of the present calculations, we propose the following decay mechanisms for both tautomers, that after vertical excitation into the optically bright  $S_1({}^1\pi\pi^*)$  excited states, the ultrafast  $S_1 \rightarrow S_0$  decays occur in four comparable reaction channels *via* four different kinds of conical intersections, all of which are responsible for the ultrafast decay found experimentally. Similar deactivation mechanisms are thus obtained for the two targeted molecules.

## Acknowledgements

This work was supported by the National Science Foundation of China (NSFC) (Grant no. 21133007) and the Ministry of Science and Technology (Grant no. 2011CB808504 and 2012CB214900). Z. L. thanks the partial support provided the CAS 100 Talent Project, NSFC (Grant Nos. 21103213 and 91233106), and the Director Innovation Foundation of CAS-QIBET.

## References

- 1 K. Röttger, R. Siewertsen and F. Temps, *Chem. Phys. Lett.*, 2012, **536**, 140–146.
- 2 J. P. Villabona-Monsalve, R. Noria, S. Matsika and J. Peón, *J. Am. Chem. Soc.*, 2012, **134**, 7820–7829.
- 3 J. Chen and B. Kohler, *Phys. Chem. Chem. Phys.*, 2012, **14**, 10677–10689.
- 4 L. B. Clark and I. Tinoco, *J. Am. Chem. Soc.*, 1965, **87**, 11–15.
- 5 V. Klenwächter, J. Drobniak and L. Augenstein, *Photochem. Photobiol.*, 1967, **6**, 133–146.
- 6 W. Voelter, R. Records, E. Bunnenberg and C. Djerassi, *J. Am. Chem. Soc.*, 1968, **90**, 6163–6170.
- 7 D. Lichtenberg, F. Bergmann and Z. Neiman, *Isr. J. Chem.*, 1972, **10**, 805–817.

- 8 H. W. Schmaller, G. Hänggi and E. Dubler, *Acta Crystallogr., Sect. C: Cryst. Struct. Commun.*, 1988, **44**, 732–736.
- 9 J. Lin, C. Yu, S. Peng, I. Akiyama, K. Li, L. K. Lee and P. R. LeBreton, *J. Phys. Chem.*, 1980, **84**, 1006–1012.
- 10 S. Gogia, A. Jain and M. Puranik, *J. Phys. Chem. B*, 2009, **113**, 15101–15118.
- 11 H. L. Barks, R. Buckley, G. A. Grieves, E. Di Mauro, N. V. Hud and T. M. Orlando, *ChemBioChem*, 2010, **11**, 1240–1243.
- 12 J. M. Berg, J. L. Tymoczko and L. Stryer, *Biochemistry*, Freeman, New York, 2010.
- 13 M. P. Callahan, K. E. Smith, H. J. Cleaves, J. Ruzicka, J. C. Stern, D. P. Glavin, C. H. House and J. P. Dworkin, *Proc. Natl. Acad. Sci. U. S. A.*, 2011, **108**, 13995–13998.
- 14 O. Plekan, V. Feyer, R. Richter, A. Moise, M. Coreno, K. C. Prince, I. L. Zaytseva, T. E. Moskovskaya, D. Y. Soshnikov and A. B. Trofimov, *J. Phys. Chem. A*, 2012, **116**, 5653–5664.
- 15 M. K. Shukla and P. C. Mishra, *J. Chem. Inf. Model.*, 1998, **38**, 678–684.
- 16 M. K. Shukla and J. Leszczynski, *J. Phys. Chem. A*, 2000, **104**, 3021–3027.
- 17 M. Fernández-Quejo, M. de la Fuente and R. Navarro, *J. Mol. Struct.*, 2005, **744–747**, 749–757.
- 18 M. K. Shukla and J. Leszczynski, *Int. J. Quantum Chem.*, 2005, **105**, 387–395.
- 19 M. K. Shukla and J. Leszczynski, *J. Phys. Chem. A*, 2003, **107**, 5538–5543.
- 20 E. Mburu and S. Matsika, *J. Phys. Chem. A*, 2008, **112**, 12485–12491.
- 21 M. E. Costas and R. Acevedo-Chávez, *J. Solution Chem.*, 2012, **41**, 864–878.
- 22 R. Wu, W. Gong, T. Liu, Y. Zhang and Z. Cao, *J. Phys. Chem. B*, 2012, **116**, 1984–1991.
- 23 C. Hampel, K. Peterson and H.-J. Werner, *Chem. Phys. Lett.*, 1992, **190**, 1–12.
- 24 K. Andersson, P.-Å. Malmqvist, B. O. Roos, A. J. Sadlej and K. Wolinski, *J. Phys. Chem.*, 1990, **94**, 5483–5488.
- 25 K. Andersson, P.-Å. Malmqvist and B. O. Roos, *J. Chem. Phys.*, 1992, **96**, 1218–1226.
- 26 J. C. Tully, *J. Chem. Phys.*, 1990, **93**, 1061–1071.
- 27 W. C. Swope, H. C. Andersen, P. H. Berens and K. R. Wilson, *J. Chem. Phys.*, 1982, **76**, 637–649.
- 28 M. Barbatti, J. Pittner, M. Pederzoli, U. Werner, R. Mitric, V. Bonacic-Koutecký and H. Lischka, *Chem. Phys.*, 2010, **375**, 26–34.
- 29 M. Barbatti, A. J. A. Aquino and H. Lischka, *Phys. Chem. Chem. Phys.*, 2010, **12**, 4959–4967.
- 30 M. Barbatti, H. Lischka, S. Salzmann and C. M. Marian, *J. Chem. Phys.*, 2009, **130**, 034305.
- 31 M. Barbatti, A. J. A. Aquino, H. Lischka, C. Schrieffer, S. Lochbrunner and E. Riedle, *Phys. Chem. Chem. Phys.*, 2009, **11**, 1406–1415.
- 32 M. Barbatti, J. J. Szymczak, A. J. A. Aquino, D. Nachtigallova and H. Lischka, *J. Chem. Phys.*, 2011, **134**, 014304.
- 33 M. Barbatti, A. J. A. Aquino, J. J. Szymczak, D. Nachtigallova and H. Lischka, *Phys. Chem. Chem. Phys.*, 2011, **13**, 6145–6155.
- 34 X. Guo and Z. Cao, *J. Chem. Phys.*, 2012, **137**, 224313.
- 35 H.-J. Werner, P. J. Knowles, R. Lindh, F. R. Manby, M. Schütz, P. Celani, T. Korona, A. Mitrushenkov, G. Rauhut, T. B. Adler, R. D. Amos, A. Bernhardsson, A. Berning, D. L. Cooper, M. J. O. Deegan, A. J. Dobbyn, F. Eckert, E. Goll, C. Hampel, G. Hetzer, T. Hrenar, G. Knizia, C. Köppl, Y. Liu, A. W. Lloyd, R. A. Mata, A. J. May, S. J. McNicholas, W. Meyer, M. E. Mura, A. Nicklass, P. Palmieri, K. Pflüger, R. Pitzer, M. Reiher, U. Schumann, H. Stoll, A. J. Stone, R. Tarroni, T. Thorsteinsson, M. Wang and A. Wolf, *MOLPRO, version, 2009.1, a package of ab initio programs*, 2009.
- 36 H. Lischka, R. Shepard, F. B. Brown and I. Shavitt, *Int. J. Quantum Chem.*, 1981, **S15**, 91–100.
- 37 H. Lischka, R. Shepard, R. M. Pitzer, I. Shavitt, M. Dallos, T. Müller, P. G. Szalay, M. Seth, G. S. Kedziora, S. Yabushita and Z. Y. Zhang, *Phys. Chem. Chem. Phys.*, 2001, **3**, 664–673.
- 38 H. Lischka, R. Shepard, I. Shavitt, R. M. Pitzer, M. Dallos, T. Müller, P. G. Szalay, F. B. Brown, R. Ahlrichs, H. J. Boehm, A. Chang, D. C. Comeau, R. Gdanitz, H. Dachsel, C. Ehrhardt, M. Ernzerhof, P. Höchtl, S. Irle, G. Kedziora, T. Kovar, V. Parasuk, M. J. M. Pepper, P. Scharf, H. Schiffer, M. Schindler, M. Schüller, M. Seth, E. A. Stahlberg, J.-G. Zhao, S. Yabushita, Z. Zhang, M. Barbatti, S. Matsika, M. Schuurmann, D. R. Yarkony, S. R. Brozell, E. V. Beck, J.-P. Blaudeau, M. Ruckebauer, B. Sellner, F. Plasser and J. J. Szymczak, *COLUMBUS, an ab initio electronic structure program, release, 7.0*, 2012.
- 39 G. Karlström, R. Lindh, P.-Å. Malmqvist, B. O. Roos, U. Ryde, V. Veryazov, P.-O. Widmark, M. Cossi, B. Schimmelpfennig, P. Neogrady and L. Seijo, *Comput. Mater. Sci.*, 2003, **28**, 222–239.
- 40 M. Barbatti, G. Granucci, M. Ruckebauer, F. Plasser, J. Pittner, M. Persico and H. Lischka, *NEWTON-X: a package for Newtonian dynamics close to the crossing seam, version 1.2*, 2011.
- 41 M. Barbatti, G. Granucci, M. Persico, M. Ruckebauer, M. Vazdar, M. Eckert-Maksic and H. Lischka, *J. Photochem. Photobiol., A*, 2007, **190**, 228–240.
- 42 R. Shepard, H. Lischka, P. G. Szalay, T. Kovar and M. Ernzerhof, *J. Chem. Phys.*, 1992, **96**, 2085–2098.
- 43 R. Shepard, in *Modern Electronic Structure Theory*, ed. D. R. Yarkony, World Scientific, Singapore, 1995, vol. 1, p. 345.
- 44 H. Lischka, M. Dallos and R. Shepard, *Mol. Phys.*, 2002, **100**, 1647–1658.
- 45 H. Lischka, M. Dallos, P. G. Szalay, D. R. Yarkony and R. Shepard, *J. Chem. Phys.*, 2004, **120**, 7322–7329.
- 46 M. Dallos, H. Lischka, R. Shepard, D. R. Yarkony and P. G. Szalay, *J. Chem. Phys.*, 2004, **120**, 7330–7339.
- 47 Z. Lan, E. Fabiano and W. Thiel, *ChemPhysChem*, 2009, **10**, 1225–1229.
- 48 B. Heggen, Z. Lan and W. Thiel, *Phys. Chem. Chem. Phys.*, 2012, **14**, 8137–8146.
- 49 B. Cohen, P. M. Hare and B. Kohler, *J. Am. Chem. Soc.*, 2003, **125**, 13594–13601.